HHS Public Access

Author manuscript

Nat Methods. Author manuscript; available in PMC 2013 May 01.

Published in final edited form as:

Nat Methods. 2012 November ; 9(11): 1113–1119. doi:10.1038/nmeth.2210.

Magnetic nanoparticle-mediated massively-parallel mechanical modulation of single-cell behavior

Peter Tseng[1,2], **Jack W. Judy**[1,2,3], and **Dino Di Carlo**[1,3,4,*]

[1]Department of Bioengineering, University of California, Los Angeles, Los Angeles, California

[2]Department of Electrical Engineering, University of California, Los Angeles, Los Angeles, California

[3]California NanoSystems Institute, University of California, Los Angeles, Los Angeles, California

[4]Jonsson Comprehensive Cancer Center, University of California, Los Angeles, Los Angeles, California

Abstract

We report a technique for generating controllable, time-varying and localizable forces on arrays of cells in a massively parallel fashion. To achieve this, we grow magnetic nanoparticle-dosed cells in defined patterns on micro-magnetic substrates. By manipulating and coalescing nanoparticles within cells, we apply localized nanoparticle-mediated forces approaching cellular yield tensions on the cortex of *HeLa* cells. We observed highly coordinated responses in cellular behavior, including the p21-activated kinase (PAK)-dependent generation of active, leading-edge type filopodia, and biasing of the metaphase plate during mitosis. The large sample size and rapid sample generation inherent to this approach allow the analysis of cells at an unprecedented rate; a single experiment can potentially stimulate tens of thousands of cells for high statistical accuracy in measurements. This technique shows promise as a tool for both cell analysis and control.

Introduction

Mechanical force plays a critical role in a large variety of cellular processes, including cell division, contractility, differentiation, and motility. The study of how cells respond to, transmit, and convert these mechanical signals into chemical signals (mechanotransduction) is a burgeoning field of science[1–3]—understanding the recurring mechanisms in cellular response to force not only enlightens us about single-cell biology, but could provide a

[*]**Author Information** Reprints and permissions information is available at www.nature.com/reprints. Correspondence and requests for materials should be addressed to dicarlo@seas.ucla.edu.

End Notes

Supplementary Information is linked to the online version of the paper.

Author Contributions P. T., and D. D., contributed to initial concept. P T. and J.W.J. contributed to the fabrication design. D.D. and P.T. designed the integration of magnetic elements and single cells. P. T. developed the final fabrication and cell patterning protocols. P.T. fabricated the micro-magnetic slides, and conducted the cell experiments. J. W. J. and P. T. discussed the FEM simulation. P. T. designed the numerical analysis flow. P.T. and D. D. discussed and analyzed the numerical results. All authors commented on the manuscript.

tangible method by which to influence cellular function. A fundamental need in the study of cellular mechanics is the on-demand local application of controlled forces over a large population of cells to obtain statistically relevant measurements of noisy biological responses.

Current approaches in which a probing instrument (e.g. atomic force microscope tip[4–6], optical and magnetic tweezers[7–10], or micropipette[11–13]) is brought in registration with a single cell are intrinsically limited by the serial nature of single-cell manipulation, and the inability to maintain spatially resolved, well-controlled stimuli for prolonged periods of time. Remote approaches, including magnetic-twisting-cytometry (MTC) and optical tweezers typically generate up to 300 pN of force, below the up to 100 nN of force generated by cells. Bulk approaches including cell stretching[14,15], micropost manipulation[16], and silicon microchips[17], although capable of generating larger forces, lack spatial resolution in mechanical stimulation and the capability of resolving a localized stimulus at the single cell level. In this work, we demonstrate a hybrid approach in which many individually patterned magnetic nanoparticle-dosed cells are brought into uniform alignment with arrays of magnetizable ferromagnetic elements[18]. Coalescing of internalized nanoparticles proximal to micro-magnetic elements with the application of an external magnetic field allows the generation of highly localized, repeatable mechanical stimuli (in excess of 100 nN, and 5 nN μm^{-1}) on the cellular cortex, resolving many of the limitations in throughput, scalability, and resolution in existing approaches. This capability comes at the cost of system complexity: substrates and magnetic nanoparticles must be specifically designed in order to achieve an optimal effect. However, designing cellular and micro-magnetic patterns gives scientists an additional layer of control over the localization and distribution of mechanical stimuli.

We found that mechanical tension mediated by localized nanoparticles in HeLa cells generates a coordinated cellular response in both local biochemistry and higher order biological processes. Applied stimuli generated substantial asymmetry in filopodia at tensions above 1 nN μm^{-1}, dependent on the activation of the mechanotransductive protein PAK. Finally, we found that asymmetric nanoparticle-mediated forces, applied throughout mitosis, can strongly bias the mitotic spindle axis in a manner that competes with extracellular adhesive cues[19].

Online Methods

Magnetic fluorescent nanoparticle preparation

A proportion of (4:2:3) of suspended dextran-magnetic nanoparticles (nanomag-D, plain –OH, Micromod), 10 M NaOH, and epichlorohydrin was reacted for 24 hours under darkness[1]. Ammonium hydroxide was then added in excess (in the same proportion as the initial nanoparticle colloid), and reacted for another 24 hours in darkness, and the final suspension was dialyzed exhaustively in DI water. The suspension was separated in multiple cycles with a permanent magnet, and finally concentrated to its approximate initial concentration in pH 8.3 bicarbonate buffer. Aminated magnetic fluorescent nanoparticles were subsequently reacted with 10 $\mu g\ ml^{-1}$ alexa fluor 647 succinimidyl ester, or alexa fluor 568 succinimidyl ester. Nanoparticles were tested for brightness and internalization, and

reacted with more fluorophore as needed (typically under 20 μg ml^{-1} total fluorophore). The suspension was again separated in multiple cycles by permanent magnet, in addition to gentle heating (55 °C) to stabilize the final colloid, before finally being suspended in PBS, and stored at 4 °C.

Fabrication of micro-magnetic slides

Polished borosilicate glass (Tech Gophers), or glass slides (Fisher) were cleaned in heated Piranha for 30 minutes, washed with DI water, and subsequently acetone, methanol and isopropanol, before finally being subjected to oxygen plasma cleaning in a barrel asher. A 30 nm Ti, 250 nm Cu, and 30 nm Ti seed layer was then evaporated onto the substrate. KMPR photoresist was spun and processed according to specification to form the electroplating mold for nickel-iron alloy. Titanium was etched in 1 % HF, and Ni_xFe_y (goal: 70:30) was electroplated in a custom plating setup (bath: NiO4x7H20 250 g L^{-1}, 5 g L^{-1} FeSO4x7H2O, 25 g L^{-1} boric Acid, 1g L^{-1} saccharin, 1 g L^{-1} sodium lauryl sulfate, pH 3.0) with a goal current density of 3 mA cm^{-2}, and a thickness of approximately 10 μm. Photoresist was stripped in Aleg 355, and the seed layer etched in copper etchant (1 % HF, 5 % Acetic Acid, 15 % H_2O_2), and titanium etchant (1 % HF). The metal layer was then passivated by deposition of 100 nm PECVD Si_xN_y. PSR photoresist (a gift from M. Bachman) was processed to optimize substrate planarity. A mix of PSR-10 and PSR-50 was spun with an acceleration of 500 rpm s^{-1}, up to an rpm to obtain desired substrate thickness (typically 2500 rpm to 3600 rpm). The substrate was baked for 1 min at 65 °C before being ramped to 95 °C within 3 minutes, and baked at 95 °C for 25 minutes, before the hotplate was turned off. The resist was subsequently exposed, post-exposure baked for 1 min 65 °C, 3 min 95 °C, and finally cured under nitrogen at 120 °C for 10 minutes. Cells were patterned using a lithographic approach[2]. AZ5214E was prebaked, exposed, and developed to form the protein pattern.

Cell preparation

HeLa cells were incubated with varying concentrations of nanoparticles (dependent on nanoparticle fabrication yield). In general, for optimally processed nanoparticles, cells are incubated in 50 μg ml^{-1} of nanoparticles in DMEM at 37 °C for 20 to 60 minutes (the final required time is dependent on the desired dosage of nanoparticles in cells—this can be approximated by eye under a microscope), before being washed aggressively in PBS, and rewashed in DMEM. Cells were allowed to recover after washing for a minimum of 2 hours before use (longer recovery times yield cleaner substrates). The average number of nanoparticles per cell (i.e. dosage)s depends on nanoparticle concentration, cell incubation time, and nanoparticle surface chemistry (Figure 5 and Supplementary Fig. 1).

Cell patterning protocol

To prepare substrates for cellular adhesion, a 40 μg mL^{-1} fibronectin and 25 μg mL^{-1} fibrinogen-alexafluor 568 solution was pipetted onto the surface and incubated for 2 hours within a petri dish. The surface was washed aggressively with PBS, and allowed to settle in PBS for 5 minutes before the protein mask was stripped in ethanol for 1 minute with two five second ultrasonic pulses. The substrate was again washed with PBS, before being

incubated in 2 % pluronic F127 (Sigma) for 50 minutes. The substrate was finally washed three times in PBS, and incubated in warm DMEM in a sterile petri dish. Prepared cells were trypsinized, pelleted, and resuspended in DMEM, and then pipetted above the substrate to achieve a goal of 10 cells per 10000 μm^2. Cell adhesion was checked at 10 minute intervals, before excess cells were washed in DMEM, and the cells were allowed to settle on the substrate for a minimum of two hours before subsequent experimentation

FACS sorting of nanoparticle-internalized cells

Cells were sorted in a BDaria II FACS sorter, using a 100 μm nozzle at 20 psi. Two separate cells populations following overnight incubation after nanoparticle dosing were either sorted by FACS or not sorted. We seeded cells from these experiments onto separate substrates and coalesced nanoparticles by permanent magnet for 2.5 hours. Samples were then imaged under fluorescence microscopy for quantification of localized nanoparticles.

Actin asymmetry experiments

A NdFeB rare earth magnet (1”x1”x1”, K&J Magnetics) was applied to the bottom of a cell-seeded, magnetic substrate-containing petri dish and the dish was incubated at 37 °C. The cells were allowed to stabilize to their final state over 4 to 5 hours, depending on the combined magnetic element and resin thickness. Control samples utilized thick substrates (4 to 5.5 μm) with cells overloaded with nanoparticles that were localized under high field for 2 hours, but had the magnet removed so that the incident field was approximately .01 or 0.025 T for 2 hours. Upon completion, the substrates were quickly washed in warm 3 % formaldehyde, and allowed to incubate in solution at 37 °C. After 10 minutes, the magnet was removed, and the substrate was washed 3 times in PBS. Cells were permeabilized in 0.5% Triton-X 100 (Sigma), washed with PBS, and incubated in 3 AU phalloidin-alexa fluor 488 conjugate for 15 minutes and washed again in PBS. Cell slides were lastly cover glass mounted in Vektashield with DAPI medium (Fisher), before being sealed with nail polish.

Antibodies and inhibitors

Antibodies to myosin-x (1:1000, Novus, cat. no 22430002), beta-integrin (2 μg mL^{-1}, Millipore, clone HM beta 1.1), phospho-PAK (ser199/201) (1:400, Millipore, cat. no 09-258) were incubated with 3 % formaldehyde fixed and Triton-X permeabilized cells overnight at 4 °C. Fascin antibody (1:100, Santa Cruz Biotechnologies, clone 55K2) was incubated with methanol-fixed cells for 1 hour at room temperature. We then incubated all samples with corresponding secondary antibody (alexa fluor 568, Invitrogen, 1:500) for 45 minutes before mounting samples in either Vektashield or SlowFade with DAPI (Invitrogen). For phospho-PAK staining saponin (0.1 %) was used instead of Triton-X 100 for permeabilization.

Streptomycin (1 mM, 2 hr-, Sigma), GSMTx-4 (25 μM, 30 min-, Sigma), EGTA (5 mM, 2 hr-, Sigma in Ca free medium), CK869[3] (30 μM, 1 hr-, Sigma), PP2 (20 μM, 1hr-, Sigma), wortmannin (750 nM, 1 hr-and again 10 min-, Sigma), ML141 (10 μM, 1hr-, Tocris), NSC23766 (100 μM, 1 hr-, Tocris), axitnib (10 nM, 1hr-, Tocris), PD98059 (50 μM, 1hr-, Sigma), dasatinib (200 nM, 1 hr-, LC Labs), and IPA-3[4] (30 μM, 30 min-, Sigma) were added to high glucose DMEM, 10 % serum, and 1 % penstrep medium at notated times

before magnet application. We then excited these samples by magnet for 1 hour to 1 hour 15 min (varying with substrate thickness), before we fixed, stained, and analyzed cells as in previous actin quantification experiments. Our inhibition experiments consisted of simultaneously running mini-groups of samples, typically 2–3 samples with added inhibitors alongside a single standard sample in normal culture medium (with or without DMSO) as the control for the group. We calculated inhibitory data as a percentage of this control response.

Cell division experiments

Before nanoparticle internalization, we synchronized *HeLa* cells by double thymidine block, and allowed these to rest for 2 hours before exposing them to nanoparticles. The protocol then followed identically to actin asymmetry experiments except approximately 1 hour before estimated onset of mitosis, external magnets were either removed or positioned away from the sample to achieve an approximately 0.025 T incident field so as to modulate the asymmetric force on the cells. Cells were inspected under the microscope for rounding, and then fixed and stained when a sufficient number of cells were rounded and dividing.

Imaging

Widefield fluorescent images were captured using a Nikon inverted fluorescent microscope with a 20x objective lens on a Photometrics Coolsnap HQ2. Stitched images were captured using NIS-elements, and subsequently extracted and cropped for subsequent analysis. Hi-speed images were captured with a Phantom Cinestream v711 camera (Vision Research) with a 40× objective running at 2000 images per second. Confocal images were captured using a Leica SP2 microscope. Live cell imaging was conducted in a fluorescent microscope-incubator setup. Substrates are inverted over a plastic spacer and clamped in place. The magnet is suspended above the substrate and media, and sample subsequently imaged.

Results

Platform information

Magnetic field gradients generated by magnetizing soft ferromagnetic micro-magnets in close proximity to patterned cells allows for the remote generation of forces via coalescence of cell-internalized magnetic nanoparticles (Fig. 1). At the core of this platform is a micro-magnetic substrate composed of: i) electroplated soft magnetic elements, ii) a biocompatible, planarized resin, and iii) lithographically-generated patterns of adhesive regions to precisely align magnetic nanoparticle-dosed cells with micro-magnets. Magnetizing these micro-magnetic elements with a permanent magnet generates arrayed magnetic potential minima that rapidly and precisely localize nanoparticles inside of cells[20–22] (Fig. 1a), yielding highly consistent, force-generating nanoparticle ensembles over arrays of uniformly shaped cells (Fig. 1b). Cell patterning can generate 10,000 to 40,000 cell patterns cm^{-2}—we typically achieved a 50–75 % fill rate for both single and multiple cells, and a 20–25 % fill rate for single cells. We additionally found that cells with internalized fluorescent nanoparticles can be sorted by fluorescence intensity with flow cytometry for improved uniformity of stimuli (Supplementary Fig. 1). The force on the cell cortex can be approximated through finite-

element modeling, and depends on a number of factors, including the volume of nanoparticles, and distance of nanoparticles from the micro-magnet in z and x directions (Fig. 1c).

We observed rapid localized assembly of nanoparticles within cells (Fig. 1d and **Supplementary Video 1**). Upon assembly, the applied magnetic field and corresponding force can be changed over time by simply adjusting the distance from the adjacent permanent magnet (Fig. 1a), or varying the incident field. The goal of this system is two-fold: 1) as a tool to probe single cell mechanics at a novel scale, and 2) as an engineering technology to remotely and controllably influence cellular activity[23–25].

Fabrication

We developed a process to fabricate functioning substrates with precise alignment between patterned cells and magnetically-active elements (Supplementary Fig. 2). Nickel-Iron alloy with a goal proportion of 70:30 (permalloy) was electroplated in a custom designed setup[26]. We extracted magnetic characteristics of the permalloy layer with a vibrating sample magnetometer (M_S = 1.13 T), and the exact plating proportions of individual samples were verified with energy dispersive x-ray spectroscopy (EDAX). We chose PSR resin—a biocompatible, low background fluorescence resin[27], as the planar contacting substrate for cells. The resin was spun on over the protruding micro-magnetic elements, and processed to achieve high planarity. Thinner resin layers (0.5 to 1.0 μm above elements) had a mild topographical variation of 300 nm over 10 μm above the magnetic edges, while thicker resin varied less than 150 nm over 15 μm. Next we accomplished cell-patterning using photolithography to allow alignment of cells with the micro-magnets (Fig. 1d). Aspects of the fabrication can be tuned to achieve varying results: for example, modifying the thickness of the resin and hence the distance of the cell from the elements scales the force while the micro-magnetic elements can be sized to be smaller and their localization varied for versatility in stimulus distribution (Fig. 1e).

Simulation and force verification

We simulated the magnetic response of individual elements in Comsol Multiphysics (Supplementary Fig. 3a), for measured fields generated from a 1 inch^3 NdFeB magnet (K&J Magnetics, field measured by magnetometer). Because the size of the magnet is comparable to the substrate length, the field varies with position along the substrate relative to the permanent magnet. These measured fields primarily vary in the normal component of the magnetic field, B_n, which decreases for elements nearer the permanent magnet center (Supplementary Fig. 3b). To determine force, magnetic field gradients were either extracted from finite-element simulation through curve fitting (Supplementary Fig. 3c) for various resin heights under the varying stimuli, or directly through the x–z variation of the field, for higher precision. We estimated combined forces on particle ensembles according to the equation:

$$F=\Sigma\,(m\nabla B), \quad (1)$$

where *m* is the saturation moment of an individual nanoparticle, and the summation is over all localized nanoparticles. This equation is modified to:

$$F = \Sigma\ k\ V(x,y)\ M_{\text{sat}}\ \mu_0^{-1} \nabla\ B(x,y,z), \quad (2)$$

where *V(x,y)* is an estimate of the volume of the nanoparticle cluster at a position, *k* is the packing volume fraction of nanoparticles, and M_{sat} is the saturation magnetization of the nanoparticles, 0.11 T (nanomag-D-plain, Micromod, conjugated to fluorophores in our lab). In comparing widefield fluorescent microscopy images with confocal images, we found that it is reasonable to assume a linear relationship between fluorescent intensity and thickness of the nanoparticle cluster—intensity of a pixel in the widefield image was closely proportional to the number of nanoparticles in that square area. We then approximated force from widefield images by summing forces at each pixel position following equation 2. Packing volume fraction *k* was estimated to be 0.6–0.8 based on electron micrographs[22].

We assessed the precision and accuracy of our generated magnetic field gradients through further finite-element simulation and experimental measurement. The precision of our finite-element-modeled gradients was assessed through simple perturbation tests of substrate parameters (Supplementary Fig. 3d). Inaccuracies in characterizing substrate parameters (cell position, magnetic element thickness, and magnetic characteristics)yield 3 to 7 % variation from the expected force. We experimentally verified the accuracy of the modeled magnetic field gradients as a function of x-y-z variation in position from the micro-magnet . We seeded magnetic beads (M_s = 0.05 T, myOne, Invitrogen) in water onto substrates, and imaged trajectories of the beads in response to an applied field (**Supplementary Video 2,** $B_t \approx 0.1$ T). This was adjusted to around half the saturating field of our elements to aid in imaging of particle motion. We determined particle velocity as a function of position and calculated the Stokes drag at each distance to determine the force[28]. Comparison between forces generated by a simulated test sphere and forces determined from experimental trajectories show excellent agreement (Supplementary Fig. 4) over the operating range of our substrates.

Nanoparticle-induced tension generates filopodia asymmetry

We first evaluated how our stimulus modified the actin distribution within cells. We investigated cells patterned to square shapes using three distinct fibronectin patterns: □, I, and X. We simultaneously incubated arrays of cells on three separate substrates, with resin thicknesses of ~0.7, 1.9, and 4.3 μm above the micro-magnetic elements, under magnetic stimulus for 4–5 hours (depending on resin thickness), and subsequently fixed and stained the cells for analysis. The three resin thicknesses, slight variations in cell position, and varying quantities of nanoparticles per cell result in a range of applied forces. Qualitatively, as we increased particle-applied forces, filopodial protrusions appeared more frequently, emanating from region to which force was applied (Fig. 2). We observed that at high stresses, nanoparticles occasionally extend and retract within dynamic protrusions (**Supplementary Video 1**). Nanoparticles additionally began to generate clear deformations in the cell membrane (**Supplementary Video 3**). The largest forces created “pull-in” instability, in which the nanoparticle clusters are pulled towards their magnetic minimum

above the magnet, drawing the cell membrane along. When this occurred, actin response diverged (Fig. 2) as cells often expelled the nanoparticles, and actin stress fibers reformed behind the nanoparticles. On rare occasions dense actin projections emanated from the area of protrusion. Cells at these extremes were not included in our quantitative analysis as there was no longer a defined tension due to destabilization of the cell membrane.

We analyzed large arrays of cells and collected quantitative data describing the effect of force magnitude on local actin protrusions (Fig. 3a). In addition, we estimated tensions and stresses at which the cell membrane yielded. We imaged magnetic substrates using fluorescence microscopy with the aid of a motorized stage, and subsequently cropped, separated, and analyzed (Supplementary Fig. 5) the resulting images for average actin protrusion asymmetry (Fig. 3b). This metric is a normalized measure of the average actin protruding from the local area stimulated by nanoparticles (per unit length), in comparison with the average actin protruding from equivalent stress-fiber edge regions without adjacent nanoparticles (for X and square structures all other edges, for I the opposite edge, Supplementary Fig. 4). As tension on the cell membrane increases a larger fraction of cells display protrusion asymmetry (Fig. 3c and Supplementary Fig. 6), which we did not observe with nanoparticles alone. Scatter plots of actin protrusion asymmetry for three respective thicknesses are notably similar (Supplementary Fig. 6a). In addition, we observed no asymmetry in cells with nanoparticle quantities 2–4 times higher than those used in force experiments and subjected to an order of magnitude lower magnetic field (Fig. 3b, Supplementary Fig. 7).

Using these large data sets, we identified additional cellular effects of force. With increasing tension, neighboring actin stress fibers would often be disrupted at the position of force application (Supplementary Fig. 6). This effect appears localized in the z-plane of the cell, and is clearer in confocal images. We defined two quantitative thresholds: i) the protrusion tension threshold at which an increased number of cells display asymmetric actin protrusions (Fig. 3c), and ii) a yield tension threshold at which nanoparticle clusters destabilized the cell membrane. Our determined protrusion thresholds of 0.5 to 2 nN μm^{-1} are consistent with the 1 nN of force generated by single pillars pulling on the cell exterior that polarize cellular biochemistry[16], while the yield thresholds are consistent with the stress applied by the leading edge of a lamellipodium during extension[6,29] (1–2 nN μm^{-2} to 10 nN μm^{-2}). We found the protrusion threshold for cells adhered to the square shape to be lower than for X and I shapes. Mechanically responsive proteins may already be recruited to the local environment near adhesive complexes interacting with the square fibronectin pattern, unlike for X and I shapes.

Filopodia are PAK-dependent

Protrusive actin structures at the site of force generation possessed biochemical characteristics of functional filopodia (Fig. 4). Protrusions stained positive for the markers fascin (Fig. 4d), myosin-X (Fig. 4e), and beta-integrin, commonly associated with active, leading-edge generated filopods[30]. We further evaluated the production of filopodia as a function of cell-adhesive pattern for three ranges of force (low, high, and near yield tension) over multiple experiments, with separate substrates, and nanoparticle-loaded cells(Fig. 4a).

Consistent with the previously described experiments, cells on I and X shapes generated a similar number of filopodia, lower than the number we observed in cells adhered to square patterns.

To characterize the origins of nanoparticle-induced filopodia, we systematically inhibited various mechanotransduction pathways. A number of stretch-activated calcium channel blockers[5], including EGTA quenching of calcium, did not produce a noticeable effect on filopodia (data not shown). We tested the normalized filopodia-generation responses to seven inhibitors of major mechanostransductive proteins: CK-869 (Arp 2/3), wortmannin (multiple)[31,32], PD98059 (extracellular-signal-regulated kinases, MEK/ERK), PP2 (Src), axitinib (multiple)[33], NSC23766 (Rac)[34], and IPA-3 (PAK)[35–37] in comparison to parallel uninhibited controls (Fig. 4b). Of the twelve inhibitors we tested, only two showed notable inhibition of the force-induced filopodia: wortmannin and IPA-3, both of which are known to affect aspects of PAK[31,32]. Wortmannin-inhibited cells showed fewer and shorter filopodia, whereas IPA-3 treatment eliminated most filopodia altogether (Fig. 4b), consistent with research on PAK inhibition[36,37]. A percentage of these treated cells (~45 %) displayed non-apoptic blebbing (Supplementary Fig. 8a). Blebbing cells displayed similarly low intensities of filopodia to those without blebbing, but we did not include these cells in our analysis.

We found that PAK localized to stress fibers and formed a distinct band along the regions of high deformation of the cellular cortex (Fig. 4c and **Supplementary Video 4**). Additionally, phospho-PAK localized to filopodia tips in cells grown on I and X patterns, and throughout filopodia on square patterns and in regions close to focal adhesions (Supplementary Fig. 8b). Overall, these data suggest that localized nanoparticle-mediated tensions lead to execution of a PAK-dependent biological program of filopodial generation that is similar in nature to filopodial generation at locations of cell adhesion and force application to the fibronectin substrate.

Forces bias metaphase plate orientation

We used our setup to manipulate the organization of DNA and subsequent cell division during mitosis. The adhesive environment has been shown to direct the spindle axis, and subsequently the chromosomal organization and division axis of cells[38,39], with extracellular force as the fundamental origin of this biasing[19]. We observed that magnetic nanoparticle-mediated forces, when magnitudes were similar to those generated by actin on the cellular cortex (10 to 100 nN), caused similar effects to extracellular cortical forces, resulting in up to 90 degree shifts in the orientation of the mitotic spindle. We stimulated synchronized cells on magnetic substrates under three conditions (continuous maximal magnetic fields, high initial field subsequently modified to a lower holding value, or eventual 0 field), fixed the cells during mitosis and analyzed them. Cells in which maximal force was applied by nanoparticles exhibited cell division axes and DNA orientation biased along the direction of force in comparison to equivalently-dosed cells in which magnetic stimulus was eventually reduced (Fig. 5 and **Supplementary Video 5**). Inhibitor treatment with PP2, which has been shown to disrupt focal adhesion kinase and thus force sensing of retraction fibers[38] did not eliminate the observed biasing (Fig. 5c).

The biasing of cell division axis and DNA orientation was more apparent for cells patterned on X and I shapes as opposed to square fibronectin patterns. For both the X and I patterns force was applied to the cell membrane in regions with no adhesive connections to the substrate, while in square patterns these forces overlap with retraction fibers (Supplementary Fig. 9). Additional force generated from nanoparticles possibly competes with retraction fiber-induced force, reducing the overall change in local cortical tension for square patterns.

Discussion

We demonstrate a technological platform capable of mechanically stimulating thousands of cells simultaneously, thereby addressing the biological noise inherent to single cell activity and allowing researchers to obtain quantitative data on the cellular response to mechanical stimuli over a range of forces. We believe this approach has potential not just as a tool to study single-cell mechanical response, but as a means of cell control, potentially through modifying cell movement, division, or differentiation. More generally, once approaches to release nanoparticles from endosomes are implemented (whether mechanically or chemically), the technique provides a platform to dynamically apply a range of localized stimuli within cells. The aminated nanoparticles used in this study can be used to bind biomolecules: the bioconjugation of proteins, nucleic acids, small molecules, or whole organelles should permit an additional range of questions concerning molecular localization and its importance in cell function to be answered.

Supplementary Material

Refer to Web version on PubMed Central for supplementary material.

Acknowledgements

This work was partially supported through the National Institutes of Health Director's New Innovator Award (1DP2OD007113). The authors would like to thank M. Bachman and N. Gunn (University of California, Irvine) for samples of PSR, J. Harrison, M. Glickman, and I. Goldberg (University of Calfornia, Los Angeles) for assistance with the permalloy electroplating bath, the UCLA Advanced Light Microscopy Spectroscopy facility for assistance with confocal microscopy, K. Lin (UCLA) for high-speed imaging assistance, I. Williams (UCLA) for running FACS sorting, and the engineers of the UCLA Nanolab for processing assistance.

References

1. Ingber DE. Tensegrity: the architectural basis of cellular mechanotransduction. Ann. Rev. of Physiology. 1997; 59:575–599.
2. Orr AW, Helmke BP, Blackman BR, Schwartz MA. Mechanisms of mechanotransduction. Dev. Cell. 2007; 10:11–20. [PubMed: 16399074]
3. Chen CS. Mechanotransduction—a field pulling together? J. Cell Sci. 2008; 121:3285–3292. [PubMed: 18843115]
4. Henderson E, Haydon PG, Sakaguchi DS. Actin filament dynamics in living glial cells imaged by atomic force microscopy. Science. 1992; 257:1944–1946. [PubMed: 1411511]
5. Charras GT, Horton MA. Single Cell Mechanotransducion and its modulation analyzed by atomic force microscope indentation. Biophysical Journal. 2002; 82:2970–2981. [PubMed: 12023220]
6. Prass M, Jacobson K, Mogilner A, Radmacher M. Direct measumrent of the lamellipodial protrusive force in a migrating cell. J. Cell Biology. 2006; 174:767–772.
7. Dai J, Sheetz MP. Mechanical properties of neuronal growth cone membranes studied by tether formation with laser optical tweezers. Biophys. J. 1995; 68:988–996. [PubMed: 7756561]

8. Wang N, Butler JP, Ingber DE. Mechanotransduction across the cell surface and through the cytoskeleton. Science. 1993; 260:1124–1127. [PubMed: 7684161]
9. Laurent VM, Henon S, Planus E, Fodil R, Balland M, Isabey D, Gallet F. Assessment of mechanical properties of adherent living cells by bead micromanipulation: Comparison of magnetic twisting cytometry versus optical tweezers. J.Biomech. Eng. 2002; 124:408–421. [PubMed: 12188207]
10. Huang H, Dong CY, Kwon H, Sutin JD, Kamm RD, So PTC. Three-dimensional cellular deformation analysis with a two-photon magnetic manipulator workstation. Biophys. J. 2002; 82:2211–2223. [PubMed: 11916876]
11. Marcy Y, Prost J, Carlier M-F, Sykes C. Forces generated during actin-based propulsion: a direct measurement by micromanipulation. Proc. Nat. Acad. Sci. 2004; 101:5992–5997. [PubMed: 15079054]
12. Hochmuth RM. Micropipette aspiration of living cells. J. Biomech. 2000; 33:15–22. [PubMed: 10609514]
13. Evans E, Ritchie K, Merkel R. Sensitive force technique to probe molecular adhesion and structural linkages at biological interfaces. Biophys. J. 1995; 68:2580–2587. [PubMed: 7647261]
14. Pelham RJ, Wang Y. Cell locomotion and focal adhesions are regulated by substrate flexibility. PNAS. 1997; 94:13661. [PubMed: 9391082]
15. Banes AJ, et al. Mechanoreception at the cellular level: the detection, interpretation, and diversity of responses to mechanical signals. Biochem Cell Biol. 1995; 73:349–365. [PubMed: 8703408]
16. Sniadecki NJ, et al. Magnetic microposts as an approach to apply forces to living cells. PNAS. 2007; 104:14553. [PubMed: 17804810]
17. Hui EE, Bhatia SN. Micromechanical control of cell-cell interactions. PNAS. 2007; 104:5722. [PubMed: 17389399]
18. Tanase M, Felton EJ, Gray DS, Hultgren A, Chen CS, Reich DH. Assembly of multicellular constructs and microarrays of cells using magnetic nanowires. Lab Chip. 2005; 5:598–605. [PubMed: 15915251]
19. Fink J, et al. External forces control mitotic spindle positiong. Nat. Cell Biol. 2011; 13:771–778. [PubMed: 21666685]
20. Gao J, Zhang W, Huang PB, Zhang Zhang, X, Xu BJ. Intracellular control of fluorescent magnetic nanoparticles. J. Amer. Chem. Soc. 2009; 130:3710–3712. [PubMed: 18314984]
21. de Vries A, Krenn B, Driel R, Kanger J. Micro Magnetic tweezers for nanomanipulation inside live cells. Biophys. J. 2005; 88:2137. [PubMed: 15556976]
22. Tseng P, Di Carlo D, Judy JW. Rapid and dynamic intracellular patterning of cell-internalized magnetic fluorescent nanoparticles. Nano. Lett. 2009; 9:3053–3059. [PubMed: 19572731]
23. Dobson J. Remote control of cellular behavior with magnetic nanoparticles. Nat. Nano. 2008; 3:139–143.
24. Mannix R, Kumar S, Cassiola F, Montoya-Zavala M, Feinstein E, Prentiss M, Ingber DE. Nanomagnetic actuation of receptor-mediated signal transduction. Nature Nano. 2007; 3:36–40.
25. Huang H, Delikanli S, Zeng H, Ferkey DM, Pralle A. Remote control of ion channels and neurons through magnetic-field heating of nanoparticles. Nat. Nano. 2010; 5:602–606.
26. Glickman M, Tseng P, Harrison J, Niblock T, Goldberg IB, Judy JW. High-performance lateral-actuating magnetic MEMS switch. JMEMS. 2011; 20:842–851.
27. Pai J-H, Wang Y, Salazar GT, Sims CE, Bachman M, Li GP, Albritton NL. A photoresist with low fluorescence for bioanalytical applications. Anal. Chem. 2007; 79:8774–8780. [PubMed: 17949059]
28. Schaffer E, Norrelykke SF, Howard J. Surface forces and drag coefficients of microspheres near a plane surface measured with optical tweezers. Langmuir. 2007; 23:3654–3665. [PubMed: 17326669]
29. Abraham VC, Krishnamurthi V, Taylor DL, Lanni F. The actin-based nanomachine at the leading edge of migrating cells. Biophys. J. 1999; 77:1721–1732. [PubMed: 10465781]
30. Berg JS, Cammer M, Chinegwundoh JO, Dale BM, Cheney RE, Greenberg S. Myosin-X is an unconventional myosin that undergoes intrafilopodial motility. Nat. Cell Biol. 2002; 4:469–477. [PubMed: 12055636]

31. Papakonststanti EV, Stournaras C. Association of PI-3 Kinase with PAK1 leads to actin phosphorylation and cytoskeletal reorganization. Mol. Biol, Cell. 2002; 13:2946–2962. [PubMed: 12181358]
32. Dharmawardhane S, Brownson D, Lennartz M, Bokoch GM. Localization of p21-activated kinase 1 (PAK1) to pseudopodia, membrane ruffles, and phagocytic cups in activated human neutrophils. J. Leukocyte Biology. 1999; 66:521–527.
33. Hahn C, Schwartz MA. Mechanotransduction in vascular physiology and atherogenesis. Nat. Rev. Molecular Cell Biology. 2009; 10:53–62. [PubMed: 19197332]
34. Tzima E, Del Pozo MA, Kiosses WB, Mohamed SA, Li S, Chien S, Schwartz MA. Activation of RAC1 by shear stress in endothelial cells mediates both cytoskeletal reorganization and effects of gene expression. The EMBO Journal. 2002; 21:6791–6800. [PubMed: 12486000]
35. Zhang H, Landmann F, Zahreddine H, Rodriguez D, Koch M, Labouesse M. A tension-induced mechanotranduction pathway promotes epithelial morphogenesis. Nature. 2011; 471:99–105. [PubMed: 21368832]
36. Delorme-Walker VD, Peterson JR, Chernoff J, Waterman CM, Danuser G, DerMardirossian C, Bokoch GM. PAK1 regulates focal adhesion strength, myosin IIA distributation, and actin dynamics to optimize cell migration. J. Cell Biol. 2011; 193:1289–1303. [PubMed: 21708980]
37. Van den Broke C, Radu M, Deruelle M, Nauwynck H, Hofmann C, Jaffter ZM, Chernoff J, Favoreel HW. Alphaherpes US3-mediated reorgnazation is mediated by group A p21-activated kinases. PNAS. 2009; 106:8707. [PubMed: 19435845]
38. Thery M, Racine V, Pepin A, Piel M, Chen Y, Sibarita J-B, Bornens M. The extracellular matrix guides the orientation of the cell division axis. Nature Cell Biology. 2005; 7:947–953. [PubMed: 16179950]
39. Thery M, Jimenez-Dalmoroni A, Racine V, Bornens M, Julicher F. Experimental and theoretical study of mitotic spindle orientation. Nature. 2007; 447:493–496. [PubMed: 17495931]

References

1. Pande AN, Kohler RH, Aikawa E, Weissleder R, Jaffer FA. Detection of macrophage activity in atherosclerosis in vivo using multichannel, high-resolution laser scanning fluorescence microscopy. J. Biomed. Optics. 2006; 11 021009.
2. Guillou H, Depraz-Depland A, Planus E, Vianay B, Chaussy J, Grichine A, Albiges-Rizo C, Block MR. Lamellipodia nucleation by filopodia depends on integrin occupancy and downstream Rac1 signaling. Exp. Cell Res. 2008; 314:478–488. [PubMed: 18067889]
3. Nolen BJ, et al. Characterization of two classes of small molecule inhibitors of Arp2/3 complex. Nature. 2009; 460:1031–1034. [PubMed: 19648907]
4. Deacon SW, et al. An isoform-selective, small-molecule inhibitor targets the autoregulatory mechanism of p21-activated kinase. Chem & Biol. 2008; 15:322–331. [PubMed: 18420139]

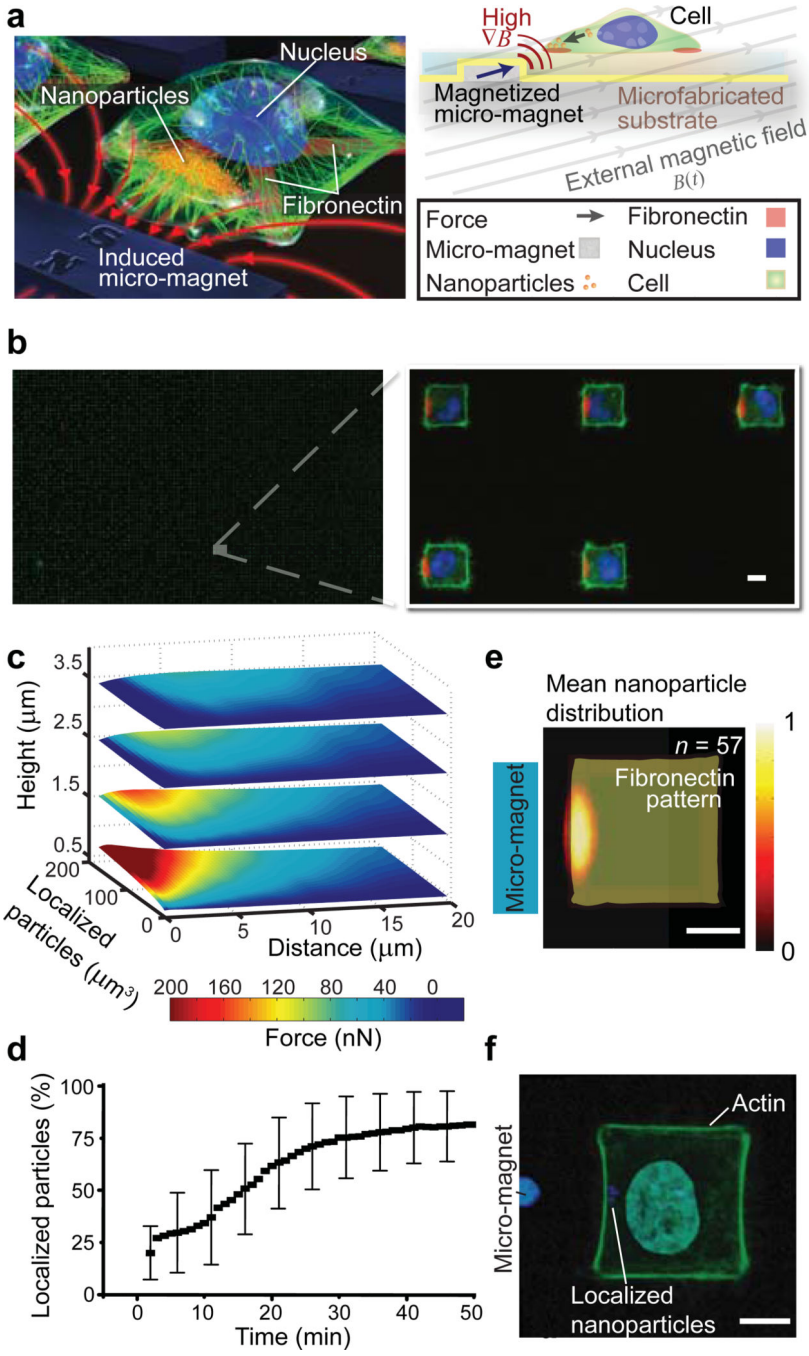

Figure 1.

Parallel dynamic localization of magnetic nanoparticle clusters within arrays of cells. (**a**) Artist's schematics of the force-generating platform. A permanent magnet remotely magnetizes soft ferromagnetic elements in proximity to fibronectin-patterned cells, coalescing magnetic nanoparticles into force-generating clusters within each cell. (**b**) Stitched images of patterned and stained cells; the right panel shows an expanded view—actin (green), nanoparticles (red), DNA (blue). (**c**) Modeled forces on the cell cortex generated by coalesced nanoparticles are plotted as a function of system parameters. Height

indicates thickness of the passivation layer above a 9.5 μm thick micro-magnet, distance indicates nanoparticle *x*-distance from the micro-magnet. The maximum internalized nanoparticle volume was around 100 μm^3, or 2 to 3 % of the total *HeLa* cell volume. The plot assumes an ideal rectangular cluster structure and an external magnetic field (B_t = 0.32, B_n = 0.075 T). (**d**) The fraction of coalescing nanoparticles (sample thickness: 0.5 μm) is plotted over time. Error bars represent standard deviation (*n* = 19 cells). (**e**) The image shows the average localization of nanoparticle ensembles (*n* = 57 cells). (**f**) The micrograph shows a single cell in which a small quantity of nanoparticles is localized with high precision by an ultra-fine magnetic tip. Scale bars, 10 μm.

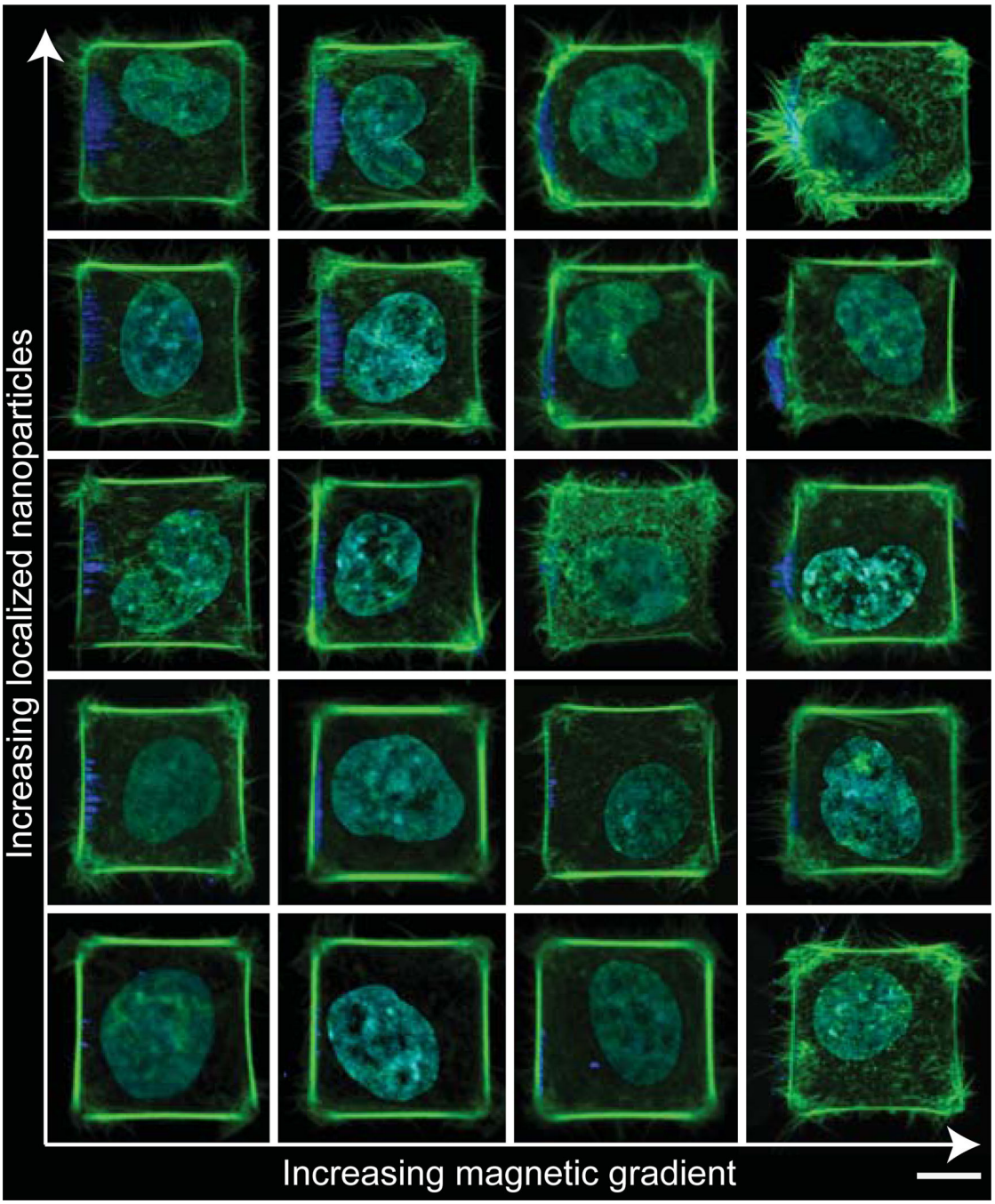

Figure 2.

Effects of magnetic field gradient and nanoparticle loading on cell response. The image shows an array of tiled cropped images of cells subject to increasing nanoparticle dose and magnetic field gradient. Cells are stained for actin (green), nanoparticles (blue), and DNA (cyan). The cells in the upper right corner display “pull-in” instability. The gradient varies from 2500 to 70000 T m^{-1}. The nanoparticle dose varies from 5 pg to 300 pg $cell^{-1}$. Scale bar is 10 μm. Note that the maximum intensity threshold for the actin channel was uniformly

reduced so that filopodia are more visually apparent. Actin protrusions are not saturated and therefore retain a linear intensity mapping.

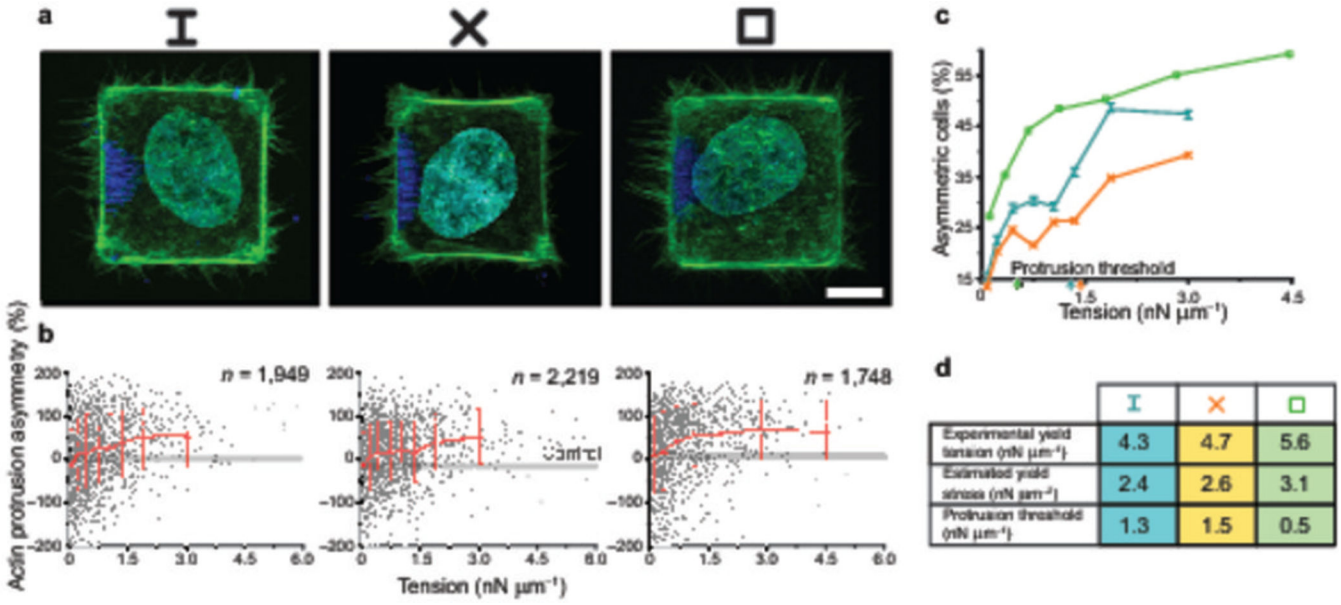

Figure 3.

Nanoparticle tension-dependent asymmetry in actin polymerization. (**a**) The images show single cells patterned using the indicated fibronectin shapes with the same colour legend as in Figure 2 (**b**) Scatter plots with overlaid averages (standard deviation represented by error bars) plotting the actin protrusion asymmetry for cells patterned by the fibronectin shapes in (a). The number of cells per sample is indicated. Zero corresponds to symmetric actin across the cell. The gray baseline in the samples is the average asymmetry as determined from control samples (excess nanoparticles under reduced magnetic field). (**c**) The graph shows the percentage of cells at a given force level with actin asymmetry over 0.7. Coloured arrows denote “protrusion thresholds,” or the tension at which this percentage nears its maximum observed for the separate fibronectin shapes (green corresponds to square, teal to I, and orange to X). (**d**) Comparison of cell yield tension (the lowest average tension at which nanoparticle clusters are observed to break through the cell membrane) on different adhesive patterns. Yield stress is estimated from yield tension and approximate nanoparticle thicknesses as obtained from confocal microscopy (1.5 to 2.3 μm, with an average of 1.8 μm). The average is used as our approximate thickness. Protrusion threshold is defined from (**c**). Scale bar is 10 μm.

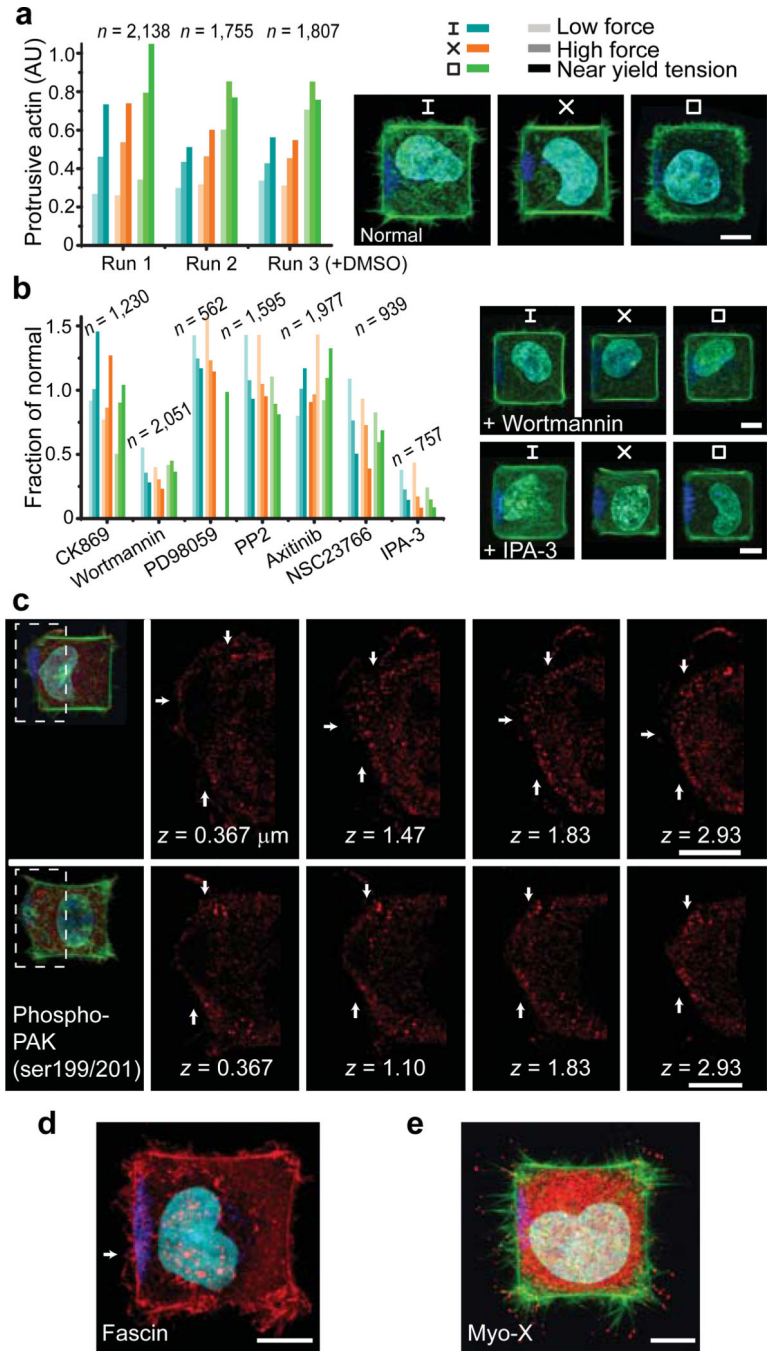

Figure 4.

Nanoparticle-mediated mechanical tension generates PAK-dependent filopodia. (**a**) The average intensity of filopodia around regions of induced tension is plotted for three experiments, for the indicated adhesion patterns. Low tension is 0– 0.15 nN µm^{-1} for square patterns and 0–0.3 nN µm^{-1} for I and X patterns. High tension is 0.15 or 0.3–2.0 nN µm^{-1}, respectively. Near yield tension is above 2 nN µm^{-1} for all patterns. The images show typical cellular responses at moderately deforming tensions. The colours are as in Figure 2. (**b**) The plots are as in (a), testing seven inhibitors of mechanotransductive proteins.

Representative images for the indicated inhibitors are shown to the right. (**c**) Z-slices through two cells with different degrees of filopodial asymmetry displaying the activation of membrane localized phospho-PAK (red). Arrows indicate a band of phospho-PAK that enfolds regions of high deformation. (**d**) and (**e**) The images show cells stained for filopodial markers fascin (d) (red, shown by arrows), myosin-x (e) (red, localized to filopodia tips), and actin (e) (green). Staining for DNA (cyan) and nanoparticles (blue) is the same in both images. Scale bars are 10 μm.

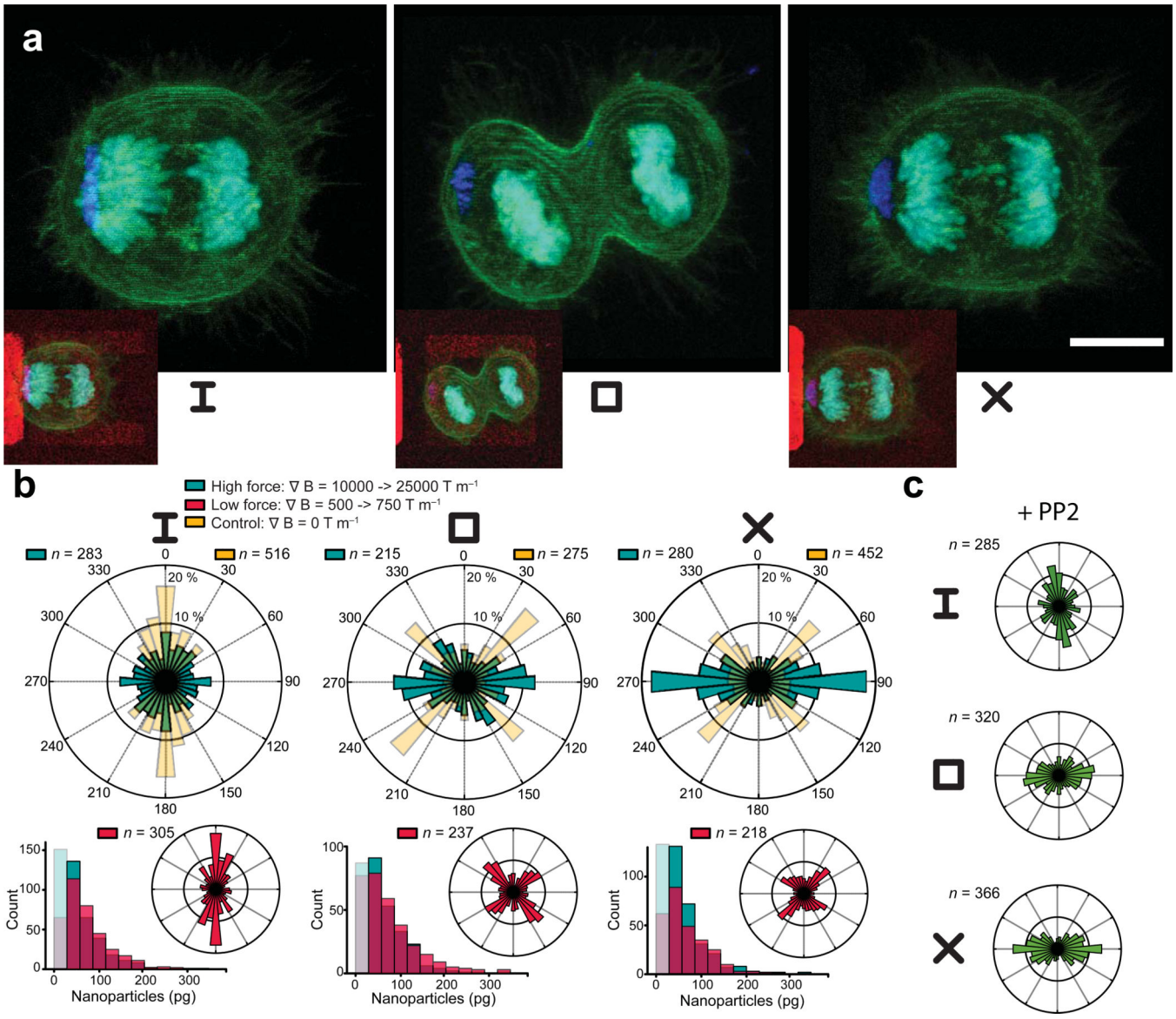

Figure 5.

Nanoparticle-mediated forces bias mitotic spindle orientation. (**a**) The images show cells dividing after adhesion on the indicated fibronectin shapes and application of force. Red signal indicates fibronectin, green signal shows actin, blue indicates nanoparticles, and cyan indicates DNA stain. (**b**) The plots show the orientation of the metaphase plate and the subsequent cell division axis for cells subject to force in comparison to control (cells with initially localized nanoparticles but no sustained force). The number of cells per sample is indicated. Shown in magenta are spindle angle histograms for control samples initially localized with nanoparticles but subsequently released to a low holding force, in conjunction with bar plots comparing the distribution of coalesced nanoparticles for both low and high applied force conditions. (**c**) The plots show orientation from samples with nanoparticle-

dosage and magnetic field stimulation as in (**b**) with inhibition of Src family kinases. Scale bar is 10 μm.